AIP | Applied Physics Letters

High-pressure Raman spectroscopy of phase change materials

Wen-Pin Hsieh, Peter Zalden, Matthias Wuttig, Aaron M. Lindenberg, and Wendy L. Mao

Citation: Applied Physics Letters **103**, 191908 (2013); doi: 10.1063/1.4829358
View online: http://dx.doi.org/10.1063/1.4829358
View Table of Contents: http://scitation.aip.org/content/aip/journal/apl/103/19?ver=pdfcov
Published by the AIP Publishing

High-pressure Raman spectroscopy of phase change materials

Wen-Pin Hsieh,[1,2,a)] Peter Zalden,[1] Matthias Wuttig,[3,4] Aaron M. Lindenberg,[1,5,6] and Wendy L. Mao[1,2]
[1]*SLAC National Accelerator Laboratory, Stanford Institute for Materials and Energy Sciences, Menlo Park, California 94025, USA*
[2]*Department of Geological and Environmental Sciences, Stanford University, Stanford, California 94305, USA*
[3]*I. Physikalisches Institut (IA), RWTH Aachen University, 52056 Aachen, Germany*
[4]*JARA – Fundamentals of Future Information Technology, RWTH Aachen University, 52056 Aachen, Germany*
[5]*Department of Materials Science and Engineering, Stanford University, Stanford, California 94305, USA*
[6]*SLAC National Accelerator Laboratory, PULSE Institute, Menlo Park, California 94025, USA*

(Received 27 September 2013; accepted 20 October 2013; published online 8 November 2013)

We used high-pressure Raman spectroscopy to study the evolution of vibrational frequencies of the phase change materials (PCMs) $Ge_2Sb_2Te_5$, $GeSb_2Te_4$, and $SnSb_2Te_4$. We found that the critical pressure for triggering amorphization in the PCMs decreases with increasing vacancy concentration, demonstrating that the presence of vacancies, rather than differences in the atomic covalent radii, is crucial for pressure-induced amorphization in PCMs. Compared to the *as-deposited* amorphous phase, the *pressure-induced* amorphous phase has a similar vibrational spectrum but requires much lower laser power to transform into the crystalline phase, suggesting different kinetics of crystallization, which may have implications for applications of PCMs in non-volatile data storage. © *2013 AIP Publishing LLC*. [http://dx.doi.org/10.1063/1.4829358]

Phase change materials (PCMs) possess many of the necessary properties for application in non-volatile electronic memory devices.[1–4] They can be cycled on nanosecond timescales[5–7] between a crystalline and an amorphous phase by applying electrical or laser pulses of appropriate intensity with the final states differing in optical reflectivity[8–10] and electrical conductivity.[9,11] This contrast in properties is caused by different bonding mechanisms in both phases and can be used to encode information and probe the present state of the memory.

$Ge_2Sb_2Te_5$ and $GeSb_2Te_4$ are the most prominent PCMs: $Ge_2Sb_2Te_5$ has been widely used in commercial electronic and optical memory devices,[12] and $GeSb_2Te_4$ with its similar properties[6] serves as an ideal prototype for calculations of properties of PCMs. They exhibit at least three different atomic arrangements: (i) The meta-stable amorphous phase prepared by melt-quenching in a device is composed of mostly Ge-Te and Sb-Te heteropolar bonds, and the atomic coordination numbers are in good agreement with the octet rule.[13,14] Since its ionicity is very small, the bonds are largely covalent.[15,16] Similar atomic arrangements are also present in the amorphous phase prepared by sputter deposition, although a minority of additional homopolar bonds is found.[17] Earlier studies on the local atomic structure of Ge atoms in the amorphous phase have led the authors to derive distinct models based on tetrahedral or distorted octahedral coordination.[18,19] Later density functional theory (DFT)-based computer simulations have shown that both local arrangements coexist[20–22] and that the Raman scattering cross sections strongly depend on the local atomic geometry,[23] therefore, preventing the quantitative discrimination of both models in experimental Raman-based studies. (ii) The meta-stable face-centered cubic rock-salt (RS) structure is obtained after crystallization at temperatures of ~100–200 °C (Ref. 6) and has one sublattice (A) entirely occupied by Te atoms, whereas the other sublattice (B) hosts the Ge and Sb atoms as well as vacancies.[24,25] The Te atoms are strongly displaced from their lattice sites, which causes both the Ge and Sb to be in defective octahedral coordination with six Te atoms, forming distinct short and long bonds.[26] (iii) The RS phase irreversibly transforms into a stable trigonal (ST) phase at higher temperature.[6] This structure with its significantly larger unit cell is best described as having alternating atomic layers of Ge, Sb, or Te, which are perpendicular to a cubic 111-direction.[27] $SnSb_2Te_4$ has the same phases as $GeSb_2Te_4$, although the atomic arrangement in its amorphous structure has not yet been investigated.

Pressure may play an important role in switching of PCM-based devices,[28] since recent high-pressure X-ray diffraction and absorption studies on $Ge_2Sb_2Te_5$ and $GeSb_2Te_4$ have shown that the initial RS phase irreversibly transforms into an amorphous phase at $P = 10$–20 GPa.[28–32] This pressure-induced amorphization is surprising, since at ambient conditions the mass density of the amorphous phase is about 8% lower than that of the RS phase.[33] The origin of the pressure-induced amorphization has been proposed to be due to different covalent sizes of the Ge and Sb atoms, which could induce an inhomogeneous strain and destabilize the lattice under pressure.[28] Alternatively, the presence of intrinsic vacancies in the crystalline lattice has also been proposed as the root cause of the amorphization.[28] The latter hypothesis is supported by DFT-based atomic relaxations in RS-$Ge_2Sb_2Te_5$ under pressure, which demonstrated that above 12 GPa, Te atoms adjacent to vacancies are displaced into neighboring vacancies,[34] where they form rotated 4-rings with three atoms from the other sublattice (Ge or Sb). This intermediate structure would give rise to a number of homopolar bonds and hence would destabilize the atomic network, finally resulting in its amorphization.

a)wphsieh@stanford.edu

Raman spectroscopy enables probing of local vibrational modes of PCMs and therefore offers a powerful means for monitoring the evolution of atomic structures during pressure-induced phase transitions that is complementary to X-ray techniques. Previous Raman studies have only been performed at ambient pressure and a conclusive assignment of Raman modes is still incomplete.[18,23,35–37] In this letter, we present high-pressure Raman spectroscopy study of the PCMs $Ge_2Sb_2Te_5$, $GeSb_2Te_4$, and $SnSb_2Te_4$. In particular, we determined the amorphization pressures for the three compounds which allow us to study the effects of vacancies and differences in atomic covalent radii on the pressure-induced amorphization. $Ge_2Sb_2Te_5$ and $GeSb_2Te_4$ have different numbers of vacancies; whereas $GeSb_2Te_4$ and $SnSb_2Te_4$ have the same nominal concentration of vacancies, only the Ge atoms have smaller covalent radii (1.20 Å) than Sn (1.39 Å), Sb (1.39 Å), and Te (1.38 Å).[38] Therefore, if the size of the smaller Ge atoms is the dominant controlling factor for the pressure-induced amorphization, then one would expect that $SnSb_2Te_4$ in which atomic sizes are approximately the same should either not amorphize or amorphize at much higher pressure than $GeSb_2Te_4$. If, on the other hand, the concentration of vacancies is the most important factor, $SnSb_2Te_4$ and $GeSb_2Te_4$ should amorphize at similar pressures. We demonstrate that the presence of intrinsic vacancies, rather than the mismatch in atomic covalent radii, is key for the pressure-induced structural transition.

Thin films of PCM with ~50 nm thickness were sputter-deposited from stoichiometric targets on a DC-operated magnetron. They were deposited on ~15 μm-thick muscovite mica substrates (grade V-1 from SPI supplies) on which $GeSb_2Te_4$ and $Ge_2Sb_2Te_5$ grew in an amorphous phase. The deposition of $SnSb_2Te_4$, however, required additional cooling of the substrate, which was facilitated by attaching a copper block cooled to −173 °C to the opposite side of the mica substrate. In order to obtain the RS phase, the specific samples were thermally annealed in a tube furnace at ~140 °C for 30 min under a continuous flow of Ar.[39,40] These RS PCMs were loaded, together with a ruby ball, into a diamond-anvil cell (DAC) with a culet size of 300 μm. The samples were compressed using methanol-ethanol mixture (4:1 in volume) as the pressure transmitting medium and the pressure was determined by ruby fluorescence.

The Raman spectra of PCMs under pressure were measured at room temperature by a Raman microscope (Renishaw) that employs a CW 514.5 nm Ar-ion laser to excite the samples and detects the Raman scattering with a spectral resolution of ~4 cm^{-1}. The cutoff frequency of the edge-filter used to exclude elastic scattering is approximately 100 cm^{-1}, below which vibrational modes are not observable by the current setup. All Raman measurements were performed using an incident laser power of 15 mW focused on the sample with a spot diameter of ~3 μm and data collection time of 6 min, except for the measurements at 0–0.15 GPa taken during *decompression* where reduced laser powers were used to avoid laser-induced recrystallization (see the discussion below). Under these excitation conditions, we did not observe thermal annealing effects that could irreversibly change the Raman spectra of the samples.

Figures 1(a) and 1(b) show the pressure dependent Raman spectra of RS-$Ge_2Sb_2Te_5$ at room temperature during the compression and decompression processes. Before compression we observe three Raman peaks at 120, 139, and 169 cm^{-1} which we denote modes *A*, *B*, and *C*, respectively. The ambient spectrum is in reasonable agreement with literature results.[18,23,35–37] The origin of the individual modes can be revealed by comparison with binary compounds in which the atoms are in the same local bonding geometry. The most similar compounds are crystalline GeTe (α-phase) and Sb_2Te_3, where Ge and Sb are equally located in distorted octahedral coordination with six neighboring Te atoms.[41–43] In GeTe, above 100 cm^{-1}, only one Raman-active mode at 132 cm^{-1} is observed.[44] In Sb_2Te_3, two Raman-active modes are present at 112 and 166 cm^{-1}, respectively.[45,46] These modes are consistent with our results and therefore we assign modes *A* and *C* with Sb-Te bonds and mode *B* with Ge-Te bonds. The association of mode *B* with Ge-Te bonds, however, requires some further discussion, since a feature similar to mode *B* was only observed in some previous Raman studies at 142 and 145 cm^{-1} (Refs. 36 and 37) and has been controversial in the literature. Some studies suggested that these modes might originate from Te-Te bonds in the amorphous[47] and even in the crystalline phase,[48] whereas other studies associated them with Ge-Te bonds. We explain in the following, why we prefer to identify the modes *B* in the RS phase with Ge-Te instead of Te-Te bonds. We follow the arguments by Němec *et al.*[37] that since Te-Te bonds in RS-GST would require a formation of anti-site defects, whose enthalpy of formation was shown to be rather high (+1.2 eV for exchanging the positions of one atom of Te and Sb[49]), Te-Te bonds are unlikely to occur in the crystalline phase. Then, why are modes similar to *B* not consistently observed in all Raman studies on RS-GST, although Ge-Te bonds are always present? The variations in the intensity of this signal are most likely related to the pronounced atomic disorder,[26] in particular around the Ge atoms, depending on the present state of thermal annealing. It is well known that a continuous atomic ordering towards the ST phase takes place in these materials[40,50] and further strongly influences the Raman scattering

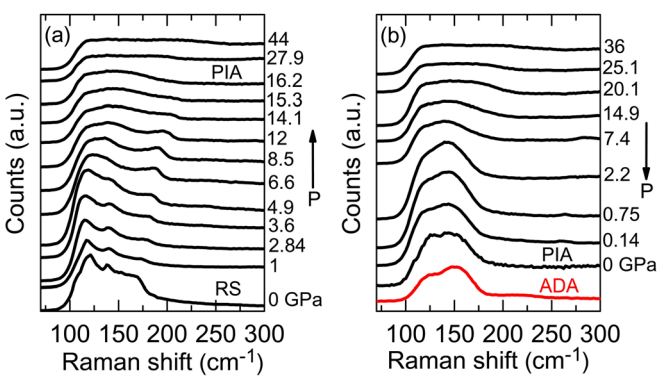

FIG. 1. Pressure dependence of the Raman spectra of RS-$Ge_2Sb_2Te_5$ during (a) compression and (b) decompression cycles. Pressure is labeled next to each spectrum which is displaced vertically for clarity. The PIA occurs at $P \approx 16.2$ GPa. The red curve in (b) shows the Raman spectrum of the ADA $Ge_2Sb_2Te_5$ at ambient pressure. During decompression, laser powers of 10 and 3 mW were used at 0.14 GPa within the DAC and 0 GPa without the DAC, respectively.

cross section of Ge-Te bonds.[23] This explains all observations on modes *B* based on well-known features of Ge-Te bonds.

Upon initial compression, the three Raman-active modes exhibit different behavior. Mode *A* slightly softens until $P = 2.84$ GPa. Mode *B* remains approximately unchanged from ambient to 4.9 GPa. In contrast, the frequency ω of mode *C* shows a pronounced pressure dependence with an increasing rate of $d\omega/dP \sim 2.42\ \mathrm{cm}^{-1}$/GPa up to 15.3 GPa. Above $P = 16.2$ GPa, distinct modes can no longer be observed, suggesting the onset of the pressure-induced amorphous (PIA) phase. The critical pressure P_c that triggers the amorphization is consistent with literature results ($P_c \sim 15$ GPa) by X-ray diffraction and absorption techniques.[28–32] Furthermore, at the highest pressure we reached, $P_m = 44$ GPa, we observe a flat spectrum consistent with a pressure-induced metallization due to the delocalization of *p* electrons in the high-pressure body-centered-cubic phase, as suggested by *ab initio* calculations.[32]

During decompression, the Raman spectra always resemble those of the PIA phase and below 2.2 GPa two broad peaks centered at $\sim$121 and $\sim 142\ \mathrm{cm}^{-1}$ are observed (Fig. 1(b)). Upon returning to ambient pressure, the spectrum of the PIA phase is very similar to that of the as-deposited amorphous (ADA) phase (red curve in Fig. 1(b)), indicating that the pressure-induced amorphization is irreversible and that the atomic bonds in PIA and ADA $Ge_2Sb_2Te_5$ are similar.

Compared to RS-$Ge_2Sb_2Te_5$, RS-$GeSb_2Te_4$ has 25% more vacancies. It displays similar vibrational spectra as a function of pressure, as shown in Fig. 2. Before compression, we observe three Raman modes at 118, 138, and 164 cm^{-1}, which we denote as modes A', B', and C', respectively. Given the similar atomic arrangements, we associate them with the same local vibrational modes as in RS-$Ge_2Sb_2Te_5$. Starting from ambient pressure, the frequency of mode A' slightly redshifts until $P = 1.3$ GPa, whereas the frequency of mode B' remains approximately unchanged up to 4.2 GPa. Mode C' again shows a significant stiffening rate of $d\omega/dP \sim 2.38\ \mathrm{cm}^{-1}$/GPa as pressure increases up to 14.3 GPa, similar to what was observed in RS-$Ge_2Sb_2Te_5$. Furthermore, the complete loss of distinct modes was observed at $P_c = 14.9$ GPa, slightly lower than the P_c of RS-$Ge_2Sb_2Te_5$ (16.2 GPa) and consistent with previous X-ray diffraction measurements.[31] This direct comparison demonstrates that with higher vacancy concentration and lower ratio of Ge to Sb atoms, the lattice stability is reduced and the crystal structure collapses at lower pressure. Note that at $P = 41$ GPa, similar to the $P_m = 44$ GPa for $Ge_2Sb_2Te_5$, we also observe a flat spectrum which suggests that a pressure-induced metallization could also occur in $GeSb_2Te_4$.

During the decompression process, the evolution of Raman spectra is also similar to that of the $Ge_2Sb_2Te_5$ (Fig. 2(b)). When returning to ambient pressure, the PIA spectrum again closely resembles that of the ADA phase. An additional Raman peak around 260 cm^{-1} is a vibrational mode of the mica substrate, which is observed most likely due to the formation of cracks in the thin film during decompression, which exposes the surface of the mica substrate to the laser light.

In RS-$SnSb_2Te_4$, all atoms are of approximately the same size and, therefore, only the intrinsic vacancies can account for the pressure-induced amorphization. Figure 3(a) presents the Raman spectra of RS-$SnSb_2Te_4$ as a function of pressure. Below 11 GPa, the RS-$SnSb_2Te_4$ shows a similar pressure dependence to the RS-$GeSb_2Te_4$ and RS-$Ge_2Sb_2Te_5$ with three Raman modes of 118, 138, and 159 cm^{-1} at ambient pressure. We refer to these modes as A'', B'', and C''. One would expect a red-shift of mode B'' as compared to the B' of RS-$GeSb_2Te_4$ due to the replacement of Ge by the heavier Sn atoms and expect an unchanged frequency of mode C'' as compared to C', which were both associated with Sb-Te vibrations. These expectations, however, are not met; the frequency of B'' is close to B' and C'' is lower than C'. These frequency shifts may arise from the inhomogeneous stress induced by differences in atomic sizes in $GeSb_2Te_4$ in which the Ge (Sb) atoms are under expansive (compressive) stress which lowers (raises) the vibrational frequency.

Upon compression mode A'' first softens until $P = 1.7$ GPa; the frequency of mode B'' remains approximately unchanged from ambient to 4 GPa. The frequency of

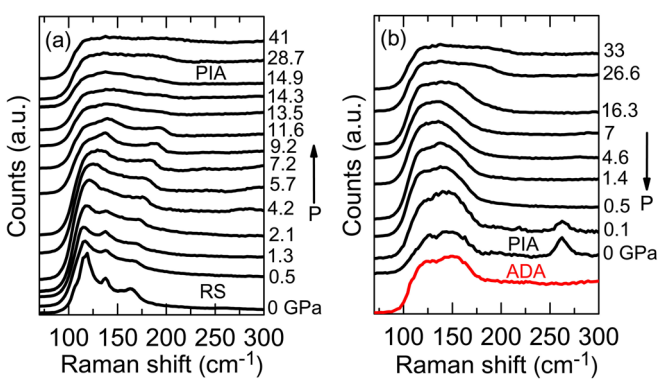

FIG. 2. Pressure dependence of the Raman spectra of RS-$GeSb_2Te_4$ during (a) compression and (b) decompression cycles. Pressure is labeled next to each spectrum which is displaced vertically for clarity. The PIA occurs at $P \approx 14.9$ GPa. Raman spectrum of the ADA $GeSb_2Te_4$ at ambient pressure (red curve in (b)) is plotted for comparison. During decompression, laser powers of 10 and 3 mW were used at 0.1 GPa within the DAC and 0 GPa without the DAC, respectively. The Raman mode at $\sim$260 cm^{-1} is due to the mica substrate.

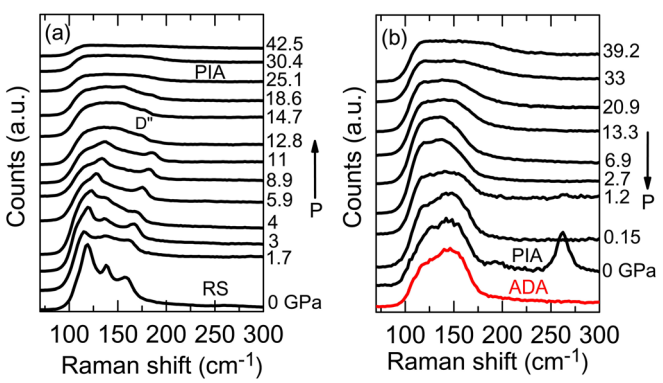

FIG. 3. Pressure dependence of the Raman spectra of RS-$SnSb_2Te_4$ during (a) compression and (b) decompression cycles. Pressure is labeled next to each spectrum which is displaced vertically for clarity. The PIA occurs above 18.6 GPa. Raman spectrum of the ADA $SnSb_2Te_4$ at ambient pressure (red curve in (b)) is plotted for comparison. During decompression, laser powers of 10 and 3 mW were used at 0.15 GPa within the DAC and 0 GPa without the DAC, respectively. The Raman mode at $\sim$260 cm^{-1} is due to the mica substrate.

TABLE I. Raman frequencies and critical pressure P_c triggering amorphization for the PCMs in this study.

	Raman frequency ω (cm^{-1}) at ambient pressure and corresponding vibrational mode			P_c (GPa)	$d\omega/dP$ of mode C before PIA (cm^{-1}/GPa)
$Ge_2Sb_2Te_5$	$\omega(A) = 120$, Sb-Te	$\omega(B) = 139$, Ge-Te	$\omega(C) = 169$, Sb-Te	16.2	2.42
$GeSb_2Te_4$	$\omega(A') = 118$, Sb-Te	$\omega(B') = 138$, Ge-Te	$\omega(C') = 164$, Sb-Te	14.9	2.38
$SnSb_2Te_4$	$\omega(A'') = 118$, Sb-Te	$\omega(B'') = 138$, Sn-Te	$\omega(C'') = 159$, Sb-Te	>18.6	2.45

mode C'' increases rapidly with increasing pressure with a rate of $d\omega/dP \sim 2.45\,cm^{-1}$/GPa up to 11 GPa. These observations allow us to conclude that before structural transformation, the modes in all three investigated compounds shift similarly with increasing pressure, in particular the change rate of modes C, C', and C''. We note that in $SnSb_2Te_4$, above 12.8 GPa, mode C'' disappears along with the appearance of an additional mode at 175 cm^{-1} (mode D'' in Fig. 3(a)). This mode then also disappears above 18.6 GPa, where no modes are discernible and the structure most likely transforms into an amorphous phase. Table I summarizes the Raman modes and critical pressure for amorphization for the PCMs we studied. Since the Raman spectrum after decompression to the ambient pressure closely resembles the spectrum of the ADA phase, see Fig. 3(b), we conclude that $SnSb_2Te_4$ also amorphizes under pressure. These results demonstrate that differences in the atomic covalent radii are not necessary for pressure-induced amorphization, supporting the crucial importance of intrinsic vacancies. However, the slightly higher P_c of $SnSb_2Te_4$ suggests that the atomic sizes may also influence the lattice stability upon compression.

The similarity of Raman spectra between the PIA and ADA phases of each PCM suggests that the local atomic arrangements might be similar in both phases – in particular since the most striking difference to the crystalline phase, namely, the broad and higher intensity Raman modes around 150 cm^{-1} is also retained in the PIA phase. On the other hand, even though their local atomic arrangements are similar, the thermal power necessary to crystallize these two amorphous phases is very different. We find that at ambient pressure, a CW laser power of ~25 mW is required to crystallize ADA $Ge_2Sb_2Te_5$ and $GeSb_2Te_4$, and ~9 mW to crystallize ADA $SnSb_2Te_4$, respectively; whereas with the same laser spot size and irradiation time, laser power of only 4–5 mW is required to crystallize all PIA samples which have been unloaded from the DAC. This finding underlines the complexity of the relationship between crystallization kinetics and atomic structure. Future studies on the possible marginal differences in the optical and structural properties, e.g., atomic coordination and chemical ordering, in the PIA and ADA phases could provide significant insights into this relationship. Furthermore, they could also help understand the structural relaxation phenomena in amorphous phases, which are responsible for the resistance drift in amorphous PCMs[51] and have to be controlled in order to increase the data storage density.[52]

The combination of micro-Raman spectroscopy with a DAC allows us to monitor the evolution of vibrational spectra of PCMs as a function of pressure. We found that the critical pressure that drives the initial crystalline structure into the amorphous phase decreases with higher concentrations of vacancies. Our results demonstrate that the vacancies, rather than differences in atomic covalent radii, play a crucial role in the pressure-induced amorphization. The Raman spectra of the PIA PCMs closely resemble those of the ADA phase. However, the PIA PCMs require significantly less incident laser intensity to crystallize, suggesting that small changes in the atomic arrangement can have a profound influence on the kinetics of the crystallization process.

This work was supported by DOE Office of Basic Energy Sciences, Materials Science and Engineering Division, under Contract DE-AC02-76SF00515. P.Z. acknowledges funding from the Alexander von Humboldt foundation.

[1]H.-S. P. Wong, S. Raoux, S. Kim, J. Liang, J. P. Reifenberg, B. Rajendran, M. Asheghi, and K. E. Goodson, Proc. IEEE **98**, 2201 (2010).
[2]M. Wuttig, Phys. Status Solidi B **249**, 1843 (2012).
[3]S. Hudgens and B. Johnson, MRS Bulletin **29**, 829 (2004).
[4]S. Raoux, W. Wełnic, and D. Ielmini, Chem. Rev. **110**, 240 (2010).
[5]G. Bruns, P. Merkelbach, C. Schlockermann, M. Salinga, M. Wuttig, T. D. Happ, J. B. Philipp, and M. Kund, Appl. Phys. Lett. **95**, 043108 (2009).
[6]N. Yamada, E. Ohno, K. Nishiuchi, N. Akahira, and M. Takao, J. Appl. Phys. **69**, 2849 (1991).
[7]S. R. Ovshinsky, Phys. Rev. Lett. **21**, 1450 (1968).
[8]M. Libera and M. Chen, J. Appl. Phys. **73**, 2272 (1993).
[9]B.-S. Lee, J. R. Abelson, S. G. Bishop, D.-H. Kang, B. Cheong, and K.-B. Kim, J. Appl. Phys. **97**, 093509 (2005).
[10]K. Shportko, S. Kremers, M. Woda, D. Lencer, J. Robertson, and M. Wuttig, Nature Mater. **7**, 653 (2008).
[11]I. Friedrich, V. Weidenhof, W. Njoroge, P. Franz, and M. Wuttig, J. Appl. Phys. **87**, 4130 (2000).
[12]M. Wuttig and N. Yamada, Nature Mater. **6**, 824 (2007).
[13]T. Matsunaga, N. Yamada, R. Kojima, S. Shamoto, M. Sato, H. Tanida, T. Uruga, S. Kohara, M. Takata, P. Zalden, G. Bruns, I. Sergueev, H. C. Wille, R. P. Hermann, and M. Wuttig, Adv. Funct. Mater. **21**, 2232 (2011).
[14]N. F. Mott, Philos. Mag. **19**, 835 (1969).
[15]D. Lencer, M. Salinga, B. Grabowski, T. Hickel, J. Neugebauer, and M. Wuttig, Nature Mater. **7**, 972 (2008).
[16]J. Kim, K. Kobayashi, E. Ikenaga, and M. Kobata, Phys. Rev. B **76**, 115124 (2007).
[17]E. Carria, A. M. Mio, S. Gibilisco, M. Miritello, F. D'Acapito, M. G. Grimaldi, and E. Rimini, Electrochem. Solid-State Lett. **14**, H480 (2011).
[18]A. V. Kolobov, P. Fons, A. I. Frenkel, A. L. Ankudinov, J. Tominaga, and T. Uruga, Nature Mater. **3**, 703 (2004).
[19]B. Huang and J. Robertson, Phys. Rev. B **81**, 081204 (2010).
[20]M. Krbal, A. V. Kolobov, P. Fons, J. Tominaga, S. R. Elliott, J. Hegedus, and T. Uruga, Phys. Rev. B **83**, 054203 (2011).
[21]S. Caravati, M. Bernasconi, T. D. Kuühne, M. Krack, and M. Parrinello, Appl. Phys. Lett. **91**, 171906 (2007).
[22]J. Akola, J. Larrucea, and R. O. Jones, Phys. Rev. B **83**, 094113 (2011).
[23]G. C. Sosso, S. Caravati, R. Mazzarello, and M. Bernasconi, Phys. Rev. B **83**, 134201 (2011).

[24]M. Wuttig, D. Lüsebrink, D. Wamwangi, W. Wełnic, M. Gillessen, and R. Dronskowski, Nature Mater. **6**, 122 (2007).
[25]T. Matsunaga and N. Yamada, Phys. Rev. B **69**, 104111 (2004).
[26]S. Shamoto, N. Yamada, T. Matsunaga, T. Proffen, J. W. Richardson, Jr., J. H. Chung, and T. Egami, Appl. Phys. Lett. **86**, 081904 (2005).
[27]T. Matsunaga, N. Yamada, and Y. Kubota, Acta Crystallogr. B **60**, 685 (2004).
[28]A. Kolobov, J. Haines, A. Pradel, M. Ribes, P. Fons, J. Tominaga, Y. Katayama, T. Hammouda, and T. Uruga, Phys. Rev. Lett. **97**, 035701 (2006).
[29]M. Krbal, A. V. Kolobov, J. Haines, A. Pradel, M. Ribes, P. Fons, J. Tominaga, C. Levelut, R. Le Parc, and M. Hanfland, Appl. Phys. Lett. **93**, 031918 (2008).
[30]M. Krbal, A. Kolobov, J. Haines, P. Fons, C. Levelut, R. Le Parc, M. Hanfland, J. Tominaga, A. Pradel, and M. Ribes, Phys. Rev. Lett. **103**, 115502 (2009).
[31]A. V. Kolobov, J. Haines, A. Pradel, M. Ribes, P. Fons, J. Tominaga, C. Steimer, G. Aquilanti, and S. Pascarelli, Appl. Phys. Lett. **91**, 021911 (2007).
[32]Y. Q. Cheng, M. Xu, H. W. Sheng, Y. Meng, X. D. Han, and E. Ma, Appl. Phys. Lett. **95**, 131904 (2009).
[33]J. Akola and R. Jones, Phys. Rev. B **76**, 235201 (2007).
[34]S. Caravati, M. Bernasconi, T. Kühne, M. Krack, and M. Parrinello, Phys. Rev. Lett. **102**, 205502 (2009).
[35]K. S. Andrikopoulos, S. N. Yannopoulos, A. V. Kolobov, P. Fons, and J. Tominaga, J. Phys. Chem. Solids **68**, 1074 (2007).
[36]R. De Bastiani, A. M. Piro, M. G. Grimaldi, E. Rimini, G. A. Baratta, and G. Strazzulla, Appl. Phys. Lett. **92**, 241925 (2008).
[37]P. Němec, V. Nazabal, A. Moreac, J. Gutwirth, L. Beneš, and M. Frumar, Mater. Chem. Phys. **136**, 935 (2012).
[38]B. Cordero, V. Gómez, A. E. Platero-Prats, M. Revés, J. Echeverría, E. Cremades, F. Barragán, and S. Alvarez, Dalton Trans. **2008**, 2832.
[39]J. Gallus, Masters thesis, FZ Jülich (available Online), 2011.
[40]T. Siegrist, P. Jost, H. Volker, M. Woda, P. Merkelbach, C. Schlockermann, and M. Wuttig, Nature Mater. **10**, 202 (2011).
[41]P. Fons, A. V. Kolobov, M. Krbal, J. Tominaga, K. S. Andrikopoulos, S. N. Yannopoulos, G. A. Voyiatzis, and T. Uruga, Phys. Rev. B **82**, 155209 (2010).
[42]T. Anderson and H. Krause, Acta Crystallogr. B **30**, 1307 (1974).
[43]P. Zalden and M. Wuttig, in Proceedings of the European\Phase Change and Ovonics Symposium, 2012.
[44]E. Steigmeier and G. Harbeke, Solid State Commun. **8**, 1275 (1970).
[45]W. Richter, H. Kohler, and C. R. Becker, Phys. Status Solidi B **84**, 619 (1977).
[46]Y. Kim, X. Chen, Z. Wang, J. Shi, I. Miotkowski, Y. P. Chen, A. L. L. Sharma, M. A. Hekmaty, Z. Jiang, and D. Smirnov, Appl. Phys. Lett. **100**, 071907 (2012).
[47]J. Tominaga and N. Atoda, Jpn. J. Appl. Phys., Part 2 **38**, L322 (1999).
[48]B. Liu, Z. T. Song, T. Zhang, S. L. Feng, and B. M. Chen, Chin. Phys. **13**, 1947 (2004).
[49]J. Zhou, Z. Sun, Y. Pan, Z. Song, and R. Ahuja, Mater. Chem. Phys. **133**, 159 (2012).
[50]W. Zhang, A. Thiess, P. Zalden, R. Zeller, P. H. Dederichs, J.-Y. Raty, M. Wuttig, S. Blügel, and R. Mazzarello, Nature Mater. **11**, 952 (2012).
[51]P. Fantini, M. Ferro, A. Calderoni, and S. Brazzelli, Appl. Phys. Lett. **100**, 213506 (2012).
[52]N. Papandreou, H. Pozidis, T. Mittelholzer, G. F. Close, M. Breitwisch, C. Lam, and E. Eleftheriou, in *Memory Workshop (IMW), 2011 3rd IEEE International* (2011), p. 1.